Mesoporous TiO_2 Films Fabricated Using Atmospheric Pressure Dielectric Barrier Discharge Jet

Hyung-Kee Seo,[†] C. Michael Elliott,*[,†] and Hyung-Shik Shin[‡]

Department of Chemistry, Colorado State University, Fort Collins, Colorado 80523-1872, United States, and School of Chemical Engineering, Chonbuk National University, Jeon-ju 561-756, South Korea

ABSTRACT TiO_2 nanoparticles were synthesized by a facile method of dielectric barrier discharge jet (DBD jet) for the dye-sensitized solar cell (DSSC) and other potential applications. DBD jet is utilized as a method for deposition of TiO_2 nanoparticles with a 9 μm/min growth rate which is more than ×25 faster than reported previously. Their performance was compared with cells fabricated using commercial TiO_2 nanoparticles (P25). The crystallinity and chemical bonding states of samples were characterized by XRD and XPS. Photoanodes fabricated by the DBD jet method resulted in approximately 50% higher photoconversion efficiency than ones prepared from P25 nanoparticles.

KEYWORDS: TiO_2 nanoparticle • atmospheric pressure plasma • dye-sensitized solar cell

INTRODUCTION

Titanium dioxide (TiO_2) is a widely investigated material used in variety of applications including photovoltaics, photocatalysis, heterojuntion solar cells, environmental purification and gas sensing (1−5). Several methods are available for TiO_2 nanoparticle synthesis including sol−gel, hydrothermal, and plasma CVD. Of these, plasma CVD is highly efficient for fabricating TiO_2 films; however, it typically requires sophisticated discharge and vacuum systems to accomplish (6, 7). Thermal plasma CVD (TPCVD) is a high-rate deposition process with control of the film's microstructure; however, the substrates can be thermally damaged, since the plasma jets irradiate the substrate directly (8). An atmospheric plasma or so-called nonthermal or low-temperature plasma requires no vacuum systems and provides higher plasma density due to the large surface/volume ratio and low-discharge current of the plasma. Hence, in recent years, considerable attention has been directed at developing versatile atmospheric-pressure technologies (9, 10). Some efforts to synthesize TiO_2 nanoparticle films by conventional plasma CVD have been reported (11−14). Of these, atmospheric pressure microplasma (sub millimeter cavity in at least one dimension) CVD has several advantages in nanoparticles synthesis compared with low-pressure plasma systems, for example, high radical densities, well-defined resultant materials, and self-organized structure (15). Because of the slow deposition rate, however, the resulting films are typically much thinner (less than 1 μm) than optimum for such applications as dye sensitized solar cell (DSSC) photoanodes (where electron diffusion lengths are in the range 10−30 μm 16−18).

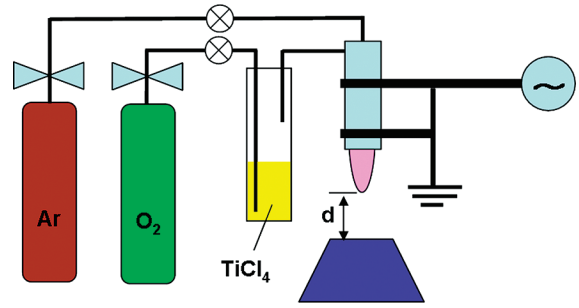

FIGURE 1. Schematic diagram of DBD jet experimental setup for TiO_2 film coating.

In this work, we report the dielectric barrier discharge jet (DBD jet) deposition onto fluorine doped tin oxide (FTO) glass of similar thickness of mesoporous TiO_2 films previously deposited using TPCVD. However, our DBD jet process results in no damage to the substrate due to indirect irradiation plasma jet unlike the TPCVD process (8). We also report faster growth rate of 9 μm/min compared to conventional plasma CVD growth rates of 0.013−0.3 μm/min (11−14). In addition, we report preliminary examinations of these materials as photoanodes in DSSC.

EXPERIMENTAL DETAILS

TiO_2 films were deposited on FTO glass substrates (Pilkington TEC glass, 15 ohm cm^{-2}) by DBD jet using $TiCl_4$ and O_2 as the precursors. The schematic of experimental apparatus used in this study is shown in Figure 1. An RF power supply having frequency of 13.56 MHz was used for generating the plasma from the middle region to the tip of the 1/4 in. diameter quartz reaction tube. O_2 (99.99%, flow rate 25 sccm) was bubbled through the $TiCl_4$ precursor and then mixed with Ar (99.99%, flow rate 6,000 sccm) in the reaction tube. These flow rates were considered base on similar experiments by Zhu et al. (14). The plasma was generated at a power of 30 W and the

* Corresponding author. E-mail: elliott@lamar.colostate.edu.
Received for review August 13, 2010 and accepted November 8, 2010
[†] Colorado State University.
[‡] Chonbuk National University.
DOI: 10.1021/am100731w
2010 American Chemical Society

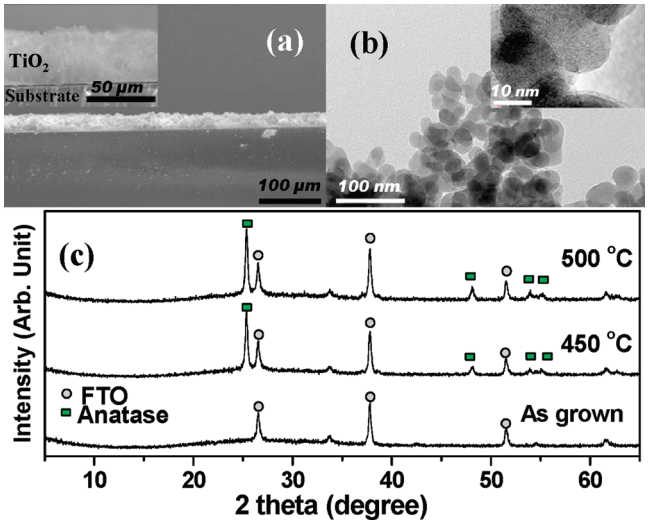

FIGURE 2. (a) FESEM and (b) TEM images of TiO_2 thin film on FTO glass, deposited by DBD jet at 30 W. The insets show the magnified images. (c) X-ray diffraction patterns of TiO_2 thin films on FTO glass deposited by DBD jet as-grown and after annealing at two different temperatures.

deposition was carried out in open air for 5 min. The TiO_2 films were deposited at a distance of 2.5 cm between the substrate and plasma tip, which produced a relatively uniform growth of the films.

The surface and transmission morphologies of TiO_2 film were examined by field emission scanning electron microscope (FESEM, JEOL JSM-6500F) and transmission electron microscope (TEM, JEOL 2010F). Information about the crystallinity of the films was obtained by Bruker D-8 X-ray diffractometer (XRD). The chemical binding states of thin films was analyzed by X-ray photoelectron electron spectroscope (XPS, PHI Multi-Technique ESCA systems).

RESULTS AND DISCUSSION

TiO_2 film deposition by DBD jet was carried out at 30 W RF power, because 20 W RF power resulted in weak plasma and 40 W RF power damaged the FTO substrate. The species present in the plasma obtained from the mixture of $Ar/O_2/TiCl_4$ gases were evaluated by optical emission spectroscopy (OES). Figure S1 in the Supporting Information shows the gaseous species identified by OES in the DBD jet. It can be seen that Ti II 337 nm and Ti I 546 nm lines originate from the fragmentation of $TiCl_4$. In addition, several Ar I lines and O I 777 and 845 nm were observed.

Figure 2 shows representative FESEM images (a), TEM images (b), and X-ray diffraction (XRD) patterns (c) of TiO_2 nanoparticle films deposited on FTO. The thickness of the deposited TiO_2 film is ca. 40 μm for the deposition time of 5 min. This deposition rate is several orders of magnitude faster than typically attainable by traditional plasma CVD, even with a low $TiCl_4$ flow rate (11, 14). Inset show the images of the TiO_2 film at higher magnification, where porous structures can be seen. The TEM images show an average nanoparticles size of ca. 25 nm for the amorphous titania. Figure 2c shows the XRD patterns of an as-deposited TiO_2 film and films annealed at 450 and 500 °C. With increasing calcination temperature the crystallite size increases from 25 to 30 nm as estimated using Scherrer's

Table 1. Element Compositions of TiO_2 Films[a]

	at %				
	O 1s	Ti 2p	C 1s	Cl 2p	N 1s
as-grown	55.7 (1.3)	21.5 (1.3)	18.1 (0.2)	4.3 (0.1)	0.5 (0.1)
450 °C	61.5 (2.8)	27.8 (1.5)	9.1 (4.6)	1.6 (0.4)	0.2 (0.2)
500 °C	60.5 (0.8)	26.4 (0.1)	12.7 (0.8)	0.4 (0.1)	0.1 (0.1)

[a] Error in parentheses is one standard deviation of mean.

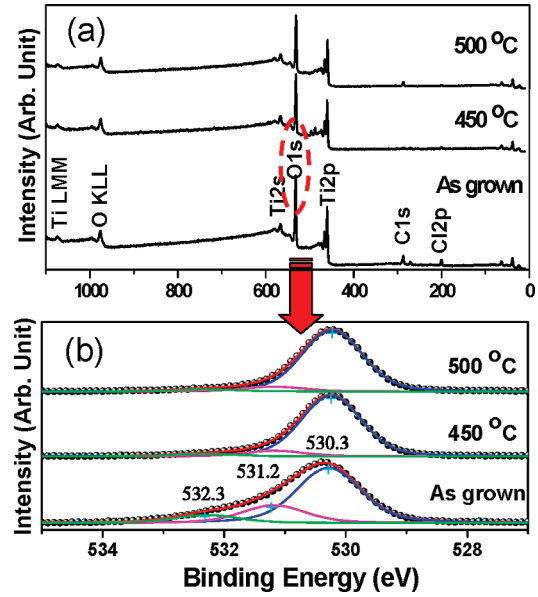

FIGURE 3. Photoelectron spectra of TiO_2 films on FTO glass deposited by DBD jet as a function of annealing temperature: (a) wide scan spectra and (b) curve fitting of high resolution O 1s.

equation applied to the anatase (101) peak (19). Interestingly, the FTO substrate appears to be important in the conversion of the amorphous, as-deposited TiO_2 material to the anatase phase. Identical films deposited by DBD jet onto glass substrates showed much lower degrees of conversion to anatase (as determined by XRD) under the same annealing conditions (i.e., time and temperature). Although the FTO layer is dimensionally stable within the annealing temperature range of 450−500 °C, the surface of soft glass begins to deform at less than 450 °C. The crystalline nature of the FTO may thus somehow be catalyzing the transition of the TiO_2 to the anatase phase; however, this is only speculation. We also investigated whether this apparent "templating" effect of the FTO might allow conversion to the anatase phase at much lower temperatures (at 200 °C); however, unfortunately, no anatase peaks were discernible in the XRD patterns of materials annealed for 10 h at this lower temperature.

TiO_2 film samples were also characterized by XPS and the percent element compositions of the surface are presented in Table 1. Particularly, it demonstrates that the percent composition of Cl 2p decrease gradually from as grown to 500 °C. N 1s composition is a negligible amount.

The spectra corresponding to Table 1 are shown in Figure 3. As can be seen in the wide scan spectra (Figure 3a), all the standard photoelectron lines of TiO_2 Ti 3p, Ti 2p, Ti 2s, O 1s and KLL, Ti LMM as well as Cl 1s, N 1s, and C 1s are

present. The peak positions of the sample were referenced with respect to carbon (C 1s) at 285.0 eV. The peak located at 200 eV is assigned as chlorine Cl 2p probably resulting from the fact that the films were prepared by decomposition of $TiCl_4$. However, this peak disappeared in the annealed films. The carbon content (determined by XPS) of the TiO_2 films are 18.1 % as prepared and 17.8, 14.9, 9.1, and 12.7 % when annealed at 200, 300, 450, and 500 °C, respectively. Thus as the annealing temperature is increased, the carbon content generally decreases. The unannealed sample yielded highest intensity of carbon signal. Some of the carbon likely is the result of organic impurities absorbed from the atmosphere prior to annealing but some may be the result carbon radicals generated from atmospheric carbon dioxide dissociation in the plasma Ti 2p XPS spectra were acquired for as-grown and annealed TiO_2 (at 450 and 500 °C). The doublet spectral line of Ti 2p for as-grown titanate is characterized by a binding energy of 458.9 eV ($2p_{3/2}$) and 464.7 eV ($2p_{1/2}$) with separation energy of 5.8 eV. Spectral lines of both the Ti $2p_{3/2}$ and $2p_{1/2}$ are similar to reported values (20−24). The small discrepancies between measured and reported binding energies are attributed to slight differences in calibration of the binding energy scales from individual instruments. In the case of annealing at 450 and 500 °C, the Ti $2p_{3/2}$ and $2p_{1/2}$ peaks are essentially the same and centered at 459 and 464.8 eV, respectively, the binding energy of Ti $2p_{3/2}$ peak is shifted to higher binding energy by 0.1 eV after annealing. These peak positions and separation, closely match the reported values for Ti^{4+} in bulk TiO_2 (22−24).

Figure 3b shows the core level O 1s XPS spectra of as grown and annealed TiO_2 (at 450 and 500 °C). Curve fitting of these spectra was carried out with Gaussian−Lorentzian distribution (70:30 ratio) and Shirley-type baseline, maintaining the chi square value less than 2. The O 1s peak can be adequately fit to three subpeaks at 530.3, 531.2, and 532.3, which are ascribed to the bulk O^{2-}, OH, and possibly O−Cl, respectively (25, 26). In the case of TiO_2, bulk oxygen in TiO_2 is assigned at 530.3 eV. In the case of as-grown titania, the O 1s subpeaks are not similar to that of annealed titania. When annealed at 450 and 500 °C, intensity of the likely O−Cl and OH binding peaks are reduced, probably because of the weak surface bond instead of strong interlayered bond. From the XPS data, it can thus be concluded that during annealing treatment, O−Cl is almost removed from the titania.

An important potential application of the materials is as DSSC photoanodes. In an effort to evaluate that potential, we have conducted preliminary comparisons of photoanodes prepared with DBD jet-deposited TiO_2 films to films prepared from commercially available P25 (Degussa) TiO_2 nanoparticles. Films were deposited as described above onto FTO glass that was masked on either side with a single layer of Scotch tape. After initial deposition, these films were planed to a uniform thickness by gently scraping the surface with a razor blade using the tape strips as spacers to determine the final thickness. Also, to match as closely as possible the conditions used in forming the P25 films, prior to annealing, the DBD jet films were coated with a solution of polyethylene glycol (PEG 2000, Sigma Aldrich) in DI water and excess solution was removed by, again, doctor-blading the surface with a razor blade (27). The coated samples were then dried at room temperature and annealed at either 450 or 500 °C for 1 h in ambient air. To prepare the films from the commercial TiO_2, we mixed the P25 with PEG solution and the resulting paste was applied to the FTO glass using the doctor blade technique but with a glass rod rather than a razor blade. After drying, these samples were annealed at 450 °C for 1 h in ambient air. Both types of mesoporous TiO_2 films (i.e., deposited by DBD jet or prepared using commercial P25 nanoparticles) were immersed overnight in an ethanol solution of *cis*-di(thiocyanato)-bis(4,4′-dicarboxy-2,2-bipyridine) ruthenium(II) (so-called N3) prepared using a modification of a procedure reported by Zhu et al. (14). Sandwich-type solar cells were assembled using the respective photoanode and a platinum-coated FTO cathode. The electrolyte solution consisted of 0.5 M LiI, 0.05 M I_2, and 0.5 M tert-butyl pyridine in γ-butyrolactone. Photocurrent density (J) and photovoltage (V) of the liquid-junction cells were measured using simulated sunlight at AM-1.5 solar emission produced by a 150 W xenon arc lamp as described previously (28). Although conditions for the measurements on the two types of photoanodes were as similar as possible, no efforts were made to optimize the cell outputs.

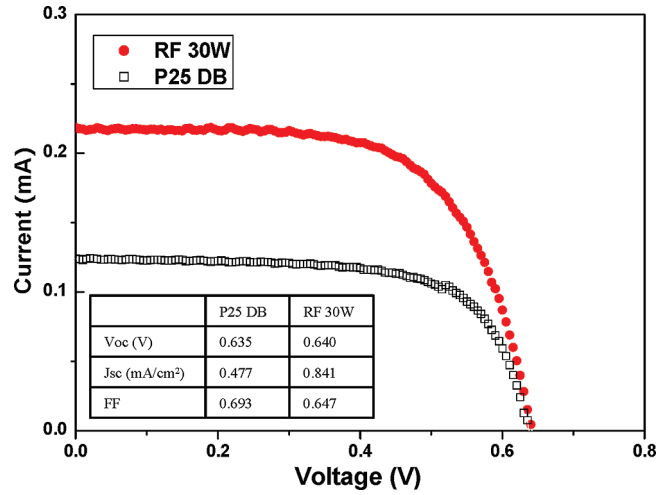

FIGURE 4. Current density−voltage responses of DSSC assembled from N3-dye photoanodes of 30 W rf-plasma fabricated sample and P25 nanoparticles TiO_2 at AM 1.5 simulated light. Both photoanodes were annealed at 450 °C.

Figure 4 provides a comparison of J-V (current density−voltage) characteristics of DSSC photoanodes. After annealing at 450 °C, the thicknesses of the DBD jet-deposited and P25 films were 4 and 5 μm, respectively (as determined by SEM). The open circuit voltage (V_{oc}) for both types of photoanodes is similar (~0.64 V), whereas the current density (J_{sc}) is almost twice as large for the DBD jet deposited film, (0.477 vs 0.841 mA/cm^2). This greater photocurrent of DBD jet deposited film may be attributable to a number of factors including minimization of charge traps and optimal oxygen vacancies (7). From our SEM images (Figure 2), however, we suggest that the higher J_{sc} of the DBD jet-deposited film

is correlated to an increased porosity and a concomitantly greater dye loading. This is consistent with the darker color observed for the dyed DBD jet films relative to the P25, despite the former being thinner.

CONCLUSIONS

In summary, the reported TiO_2 films were deposited at 30 W RF power by a DBD jet using $TiCl_4/O_2$ as precursors and argon as a plasma generation gas. The suggested method can be easily adopted for fabrication of TiO_2 films on FTO glass at rates that are more than ca. 25 times faster than previously reported plasma CVD. Employing these films as mesoporous photoanodes in DSSC, there is a ~50% improvement in photoconversion efficiency relative to comparable photoanodes fabricated from commercial TiO_2 nanoparticles (P25, Degussa). Finally, the DBD jet method has several times larger deposition area than microplasma; however, the synthesis area is not large enough for commercialization. However, it should be possible to engineer multiplasma jet and/or slot-microplasma designs to scale up for large area synthesis.

Acknowledgment. This work was supported by the Chemical Science, Geosciences and Bioscience Division, Office of Basic Energy Sciences, Office of Science, U.S. Department of Energy (DE-FG02-04ER15591), and the Korea Research Foundation Grant funded by the Korean Government (MOE-HRD) KRF-2007-357-D00066.

Note Added after ASAP Publication. This paper was published on the Web on November 11, 2010, with minor text errors. The corrected version was reposted on November 16, 2010.

Supporting Information Available: Figure S1 shows the optical emission spectrum of $Ar/O_2/TiCl_4$ gases mixture at 30 W RF power (PDF). This material is available free of charge via the Internet at http://pubs.acs.org/.

REFERENCES AND NOTES

(1) Hoffmann, M. R.; Martin, S. T.; Choi, W.; Bahnemann, D. W. *Chem. Rev.* **1995**, *95*, 69.
(2) Kim, K. J.; Benksten, K. D.; Lagemaat, J. V.; Frank, A. J. *Chem. Mater.* **2002**, *14*, 1042.
(3) Wang, R.; Hashimoto, K.; Fujishima, A. *Nature* **1997**, *388*, 431.
(4) Grätzel, M. *J. Photochem. Photobiol. A: Chem.* **2004**, *164*, 3.
(5) Grätzel, M. *Prog. Photovolt.* **2006**, *14*, 429.
(6) Busani, T.; Devine, R. A. B. *Semicond. Sci. Technol.* **2005**, *20*, 870.
(7) Sharma, R.; Das, P. P.; Misra, M.; Mahajan, V.; Bock, J. P.; Trigwell, S.; Biris, A. S.; Mazumder, M. K. *Nanotechnology* **2009**, *20*, 75704.
(8) Ando, Y. *IEEE Trans. Plasma Sci.* **2009**, *37*, 2202.
(9) Yan, X.; Zou, F.; Lu, X. P.; He, G.; Shi, M. J.; Xiong, Q.; Gao, X.; Xiong, Z.; Li, Y.; Ma, F. Y.; Yu, M.; Wang, C. D.; Wang, Y.; Yang, G. *Appl. Phys. Lett.* **2009**, *95*, 083702.
(10) Shashurin, A.; Keidar, M.; Bronnikov, S.; Jurjus, R. A.; Stepp, M. A. *Appl. Phys. Lett.* **2008**, *93*, 181501.
(11) O'Neill, S. A.; Parkin, I. P.; Clark, R. J. H.; Mills, A.; Elliott, N. *J. Mater. Chem.* **2003**, *13*, 56.
(12) Di, L. B.; Li, X. S.; Shi, C.; Xu, Y.; Zhao, D. Z.; Zhu, A. M. *J. Phys. D: Appl. Phys.* **2009**, *42*, 32001.
(13) Yoshiki, H.; Saito, T. *J. Vac. Sci. Technol., A* **2008**, *26*, 338.
(14) Zhu, A. M.; Nie, L. H.; Wu, Q. H.; Zhang, X. L.; Yang, X. F.; Xu, Y.; Shi, C. *Chem. Vap. Deposition* **2007**, *13*, 141.
(15) Mariotti, D.; Sankaran, R. M. *J. Phys. D: Appl. Phys.* **2010**, *43*, 21.
(16) Nazeeruddin, M. K.; Angelis, F. D.; Fantacci, S.; Selloni, A.; Viscardi, G.; Liska, P.; Ito, S.; Takeru, B.; Grätzel, M. *J. Am. Chem. Soc.* **2005**, *127*, 16835.
(17) Nazeeruddin, M. K.; Kay, A.; Rodicio, I.; Humphry-Baker, R.; Müller, E.; Liska, P.; Vlachopoulos, N.; Grätzel, M. *J. Am. Chem. Soc.* **1993**, *115*, 6382.
(18) Fisher, A. C.; Peter, L. M.; Ponomarev, E. A.; Walker, A. B.; Wijayantha, K. G. U. *J. Phys. Chem. B.* **2000**, *104*, 949.
(19) Klug, H. P.; Alexander, L. E. *X-Ray Diffraction Procedures for Polycrystalline and Amorphous Materials*; John Wiley & Sons: New York, 1954.
(20) Yoshida, R.; Suzuki, Y.; Yoshikawa, S. *Mater. Chem. Phys.* **2005**, *91*, 409.
(21) Erdey, L. *Gravimetric Analysis*; Pergamon: New York, 1965, p459.
(22) Södergren, S.; Rensmo, H. S.; Lindström, H.; Hagfeldt, A.; Lindquist, S. *J. Phys. Chem. B* **1997**, *101*, 3087.
(23) Yu, J. G.; Yu, H. G.; Cheng, B.; Zhai, X. J.; Yu, J. C.; Ho, W. K. *J. Phys. Chem. B* **2003**, *107*, 13871.
(24) Seo, H. K.; Kim, G. S.; Ansari, S. G.; Kim, Y, S.; Shin, H. S.; Shim, K. H.; Suh, E. K. *Sol. Energy Mater. Sol. Cells* **2008**, *92*, 1533.
(25) Erdem, B.; Hunsicker, R. A.; Simmons, G. W.; Sudol, E. D.; Dimonie, V. L.; El-Aasser, M. S. *Langmuir* **2001**, *17*, 2664.
(26) Moulder, J. F.; Stickle, W. F.; Sobol, P. E.; Bomben, K. D. *Handbook of X-ray Photoelectron Spectroscopy*; Chastian, J., Ed.; Perkin-Elmer: Eden Prairie, MN, 1992.
(27) Kim, G. S.; Seo, H. K.; Godbole, V. P.; Kim, Y. S.; Yang, O. B.; Shin, H. S. *Electrochem. Commun.* **2006**, *8*, 961.
(28) Shawn, S. S.; Elliott, C. M.; Contado, C.; Caramori, S.; Bignozzi, C. A. *J. Am. Chem. Soc.* **2002**, *124*, 11215.

AM100731W